Flexible and Printed Electronics

PAPER

Monolithic integration of display driver circuits and displays manufactured by screen printing

Peter Andersson Ersman[1], **Marzieh Zabihipour**[2], **Deyu Tu**[2], **Roman Lassnig**[1], **Jan Strandberg**[1], **Jessica Åhlin**[1], **Marie Nilsson**[1], **David Westerberg**[1], **Göran Gustafsson**[1], **Magnus Berggren**[2], **Robert Forchheimer**[3] and **Simone Fabiano**[2]

[1] RISE Acreo, Department of Printed Electronics, Bredgatan 33, SE-602 21 Norrköping, Sweden
[2] Laboratory of Organic Electronics, Department of Science and Technology, Linköping University, SE-601 74 Norrköping, Sweden
[3] Information Coding Group, Department of Electrical Engineering, Linköping University, SE-581 83 Linköping, Sweden

E-mail: peter.andersson.ersman@ri.se **and** simone.fabiano@liu.se

OPEN ACCESS

RECEIVED
8 November 2019

REVISED
12 February 2020

ACCEPTED FOR PUBLICATION
27 February 2020

PUBLISHED
24 March 2020

Keywords: organic electrochemical transistors, organic electrochromic displays, screen printing, monolithic integration

Supplementary material for this article is available online

Abstract

Here, we report all-screen printed display driver circuits, based on organic electrochemical transistors (OECTs), and their monolithic integration with organic electrochromic displays (OECDs). Both OECTs and OECDs operate at low voltages and have similar device architectures, and, notably, they rely on the very same electroactive material as well as on the same electrochemical switching mechanism. This then allows us to manufacture OECT-OECD circuits in a concurrent manufacturing process entirely based on screen printing methods. By taking advantage of the high current throughput capability of OECTs, we further demonstrate their ability to control the light emission in traditional light-emitting diodes (LEDs), where the actual LED addressing is achieved by an OECT-based decoder circuit. The possibility to monolithically integrate all-screen printed OECTs and OECDs on flexible plastic foils paves the way for distributed smart sensor labels and similar Internet of Things applications.

1. Introduction

A vast array of novel flexible electronics, including many different kinds of electronic components, are continuously being proposed, explored and reported by the industry and the scientific community [1]. For example, applications such as energy harvesting, energy storage, addressing and computing via logic circuits, bioelectronics and display indicators have attracted a considerable attention as they offer a pathway to distribute information technology onto things and into all kinds of services of our daily life [2–6]. The resulting electronic devices are often manufactured through a combination of different processing techniques, e.g. coating, printing, thermal evaporation and photolithography [7]. However, to truly enable these applications into actual commercial products, such as devices realized on graphical surfaces and packages, it is imperative to refine the academic results into more simplified and unified manufacturing approaches. This can, for example, be obtained by combining electronic devices that are manufactured in a compatible manner, which sets the subject of the present study.

Printed flexible displays are a cornerstone of printed electronics as they allow a communication interface to visualize information and to make data-driven decisions. For this reason, they have attracted a growing interest among the academic and industrial communities [8–11]. In traditional organic electroluminescent displays, transparent conductive oxides (TCOs), such as indium tin oxide, are typically used as the electrode materials to facilitate charge injection into the organic electroluminescent layer while simultaneously maintaining high transparency [12]. The drawback is that TCOs are expensive and typically incompatible with room temperature manufacturing processes [13]. In addition, organic electroluminescent displays suffer from poor air stability of the organic molecules as well as relatively high operation voltages [14]. Unlike traditional electroluminescent displays, organic electrochromic displays (OECDs) rely on the use of

intrinsically conducting polymers which act simultaneously as the electrode and electrochromic materials, such that TCOs can be omitted [6, 11]. This is an important step that allows for a simplified and low-cost manufacturing approach of the electronic display devices in large volumes by using screen printing as the sole deposition technique. In addition to being easily manufactured from solution, OECDs allow for low operation voltage, which make them ideal candidates for heavily distributed printed display technologies [6, 11]. There exist many different OECD architectures, that can be manufactured by combining a variety of different materials [15–17]. The printed OECDs reported herein are based on oxidized poly (3,4-ethylenedioxythiophene) (PEDOT) which is chemically stabilized by the non-conjugated polyelectrolyte poly(styrenesulfonate) (PSS). This material combination yields a polymer (PEDOT:PSS) with a relatively high mixed ionic and electronic conductivity as well as pronounced electrochromism [6, 11, 17, 18]. The resulting OECDs are obtained by combining PEDOT:PSS, acting as the color changing electrode, with a counter electrode material (e.g. PEDOT:PSS or carbon), as well as with an electrolyte sandwiched between the two electrodes to facilitate electrochromic switching upon application of a voltage. Nevertheless, similarly to other display technologies, one drawback of printed OECDs is that they are susceptible to cross-talk, such that passive matrix addressing of individual pixels becomes troublesome [18, 19]. This can be solved by addressing each pixel with a transistor in printed active-matrix displays [20, 21].

Active matrix addressed OECDs, that utilize all-screen printed field-effect transistors (FETs) based on carbon nanotubes, have been reported by Cao *et al* [10]. However, since the transistors functioned in the field-effect mode, a relatively high voltage (±5 V) was required to properly operate them. In this respect, organic electrochemical transistors (OECTs) is a favorable choice before the organic FETs because of their capability to deliver higher current throughput. This is due to the fact that charges in OECTs are accumulated and transported throughout the entire bulk of the channel material, which results in current densities that are orders of magnitude higher than those typically attained in FETs [22, 23] for the same channel length/width dimensions. This property makes the OECT technology suitable for display driver applications, where high current throughput is typically needed. A drawback of the volumetric channel charging in OECTs is the relatively slower response time, as compared to FETs. However, since both OECDs and OECTs rely on similar device architectures and the same switching mechanism, they are intrinsically compatible with each other in many applications. Typically, the OECT switching time is at least one order of magnitude faster than that of the OECD. This is due to the relatively larger area of the display segments as compared to the OECT channel [6, 11]. This, together with the high current throughput, further justifies the compatibility of the two devices.

Here, we demonstrate all-screen printed OECT-based display driver circuits operated at low voltages, and their monolithic integration [24–26] with OECDs. PEDOT:PSS is here used as the exclusive electroactive material, both as the channel in the OECT and as the electrochromic layer of the OECD. The immediate advantage of this is the possibility to manufacture both devices in a concurrent screen printing process. Hence, this enables all-printed display drivers capable of updating relatively simple OECD indicators, which paves the way for flexible smart sensor labels and akin devices that has the potential to further promote the use and implementation of Internet of Things (IoT) applications.

2. Methods

2.1. Materials

OECTs and OECDs were printed on polyethylene terephtalate (PET), Polifoil Bias purchased from Policrom Screen. The transistor channel, the gate electrode, the color changing electrode of the electrochromic display, and sometimes also the counter electrode of the electrochromic display, are all based on PEDOT:PSS (Clevios SV3 purchased from Heraeus). A screen printable and UV-curable electrolyte, AFI VV009 provided by RISE Acreo, was used to enable the respective device switching mechanism. A graphite-based screen printing ink, 7102 purchased from DuPont, was used to deposit the source and drain electrodes as well as the printed resistors. A screen printing ink consisting of silver flakes, Ag 5000 purchased from DuPont, was used to lower the resistance in, e.g. probe pads and interconnects. A UV-curable ink, 5018 purchased from DuPont, was used to isolate different layers from each other.

2.2. Manufacturing of OECTs and OECDs

The multilayered device architectures were manufactured on PET substrates by using a flatbed sheet-fed screen printing equipment (DEK Horizon 03iX) with a process alignment capability of +/−25 μm. The screen printing tools were based on standard polyester threads.

The mesh counts of the set of screen printing tools were varied from 75 to 150 threads cm^{-1}, and the thread diameters were varied from 20 to 50 μm. The print gap and squeegee pressure varied between 2 and 5 mm and 10 and 20 kg, respectively, and the squeegee angle was ~65°. Seven screen printing steps were required to complete the devices. The sequence of the printing process has been described in a previous report [27], and it is also outlined below. Silver is printed as the first layer, to provide probe pads and interconnect wires. PEDOT:PSS is printed as the second layer, to form OECT channels and OECD color

changing electrodes, and carbon is subsequently printed as OECT source and drain electrodes and resistors. All three inks are dried at 120 °C for 5 min. An insulating layer is then screen printed and UV-cured. The purpose of this layer is to define the area of the subsequently deposited electrolyte layer required in both OECTs and OECDs, as well as to provide for interconnects. The electrolyte is screen printed according to the areas predefined by the insulating layer and cured through UV light irradiation. PEDOT:PSS is screen printed on the electrolyte patterns to form OECT gate electrodes and OECD counter electrodes. The interconnects are completed by bridging the insulating layer with yet another silver layer. Push buttons were used to allow for reconfiguration of the OECTs used to control the switching direction of the OECD in the monolithically integrated display driver circuit, without affecting the color state until the button is pushed, cf an enable signal. The push button, which was obtained by lamination of an adhesive silver layer on top of the previously deposited silver layer in an eighth processing step, was activated by bringing the two printed silver layers in contact with each other (short-circuit), while deactivation was obtained by separating the two printed silver layers (open-circuit).

The requirements on thickness and roughness of the printed features are not as crucial when manufacturing OECDs and OECTs, as compared to e.g. FETs manufacturing, and this is also the reason for choosing relatively coarse screen printing as the manufacturing method. The desired device functionality will be obtained as long as the electrolyte is brought into contact with its two corresponding electrodes. Due to this, the screen printing inks were printed without further optimization. The following approximate thickness and roughness values were obtained (Sensofar PLu neox optical profilometer) upon printing the inks on a PET substrate: PEDOT:PSS 0.5 μm and 0.03 μm, carbon 9 μm and 0.8 μm, silver 11 μm and 1.9 μm, insulator 15 μm and 0.4 μm, and electrolyte 13 μm and 1.1 μm. Printing of the PEDOT:PSS layer is the most critical deposition step in OECT and OECD manufacturing; a thick and/or non-uniform PEDOT:PSS layer would result in slow and/or non-reproducible switching characteristics. But as indicated by the thickness and roughness values obtained by optical profilometry, this layer is both relatively thin and smooth.

2.3. Device characterization

All measurements were performed at a temperature of ~20 °C and a relative humidity of ~45%RH. Transfer and dynamic switch measurements of the OECTs were performed by using a semiconductor parameter analyzer (HP/Agilent 4155B) and a function generator (Agilent 33120 A). The printed display driver circuits were characterized by using a data acquisition card (DAQ card PCI-6723 from National Instruments). The voltage supply, to update the respective OECD, was either +/−3 V or 1.5 V (coloration) and 0 V (bleaching). The input signals to control the conduction state of the OECTs in the printed display driver circuits were supplied by the DAQ card, at an appropriate frequency.

3. Results

3.1. Transistor designs

The OECT channel dimensions are one of the most critical design parameters, since these dictate current throughput, switching voltage and switching time of the resulting transistor. Therefore, the display driver circuits described below have been evaluated with two different OECT channel geometries, (a) either with a width (W) of 100 μm and a length (L) of 100 μm, and also (b) with W and L equal to 1000 μm and 100 μm, respectively. Note that the stated channel dimensions are according to the design of the screen printing tools, the actual dimensions of the printed channel may differ due to e.g. ink spreading, see figure S1 available online at stacks.iop.org/FPE/5/024001/mmedia. A wider OECT channel results in a much larger current throughput, for a given constant channel length, between the source and drain electrodes. The two different channel dimensions, used herein, thus differ by a factor of ten in terms of channel resistance, i.e. the 1000 × 100 μm OECT channel exhibits the lowest resistance. This is evidenced when comparing the transfer characteristics of the two OECTs (see figure 1(a)), upon application of a constant drain-source voltage (V_{DS}) of −1 V and by sweeping the gate voltage (V_{GS}) from 0 to 1.5 V. An OECT SPICE model [27] is employed to simulate the transfer curves for both channel widths (W = 1000 μm or 100 μm) and the results are reported in figure 1(b). In terms of ON/OFF ratio and switching threshold voltage, the simulation results generated by the SPICE model are in good agreement with the measured transfer characteristics of both OECTs. The model was then further used to simulate the display driver circuits presented herein.

The OECT channel dimensions also have an impact on the dynamic switching characteristics of the OECTs. This type of electrolyte-gated transistor devices exhibit switching characteristics similar to an electrochemical supercapacitor. Hence, the charge capacity, which is determined by the volume of the PEDOT:PSS serving as the channel, affects the OECT switching time (figures 1(c)–(d)). The current modulation in the OECT with the narrow (100 μm, figure 1(e) left) channel shows sharper transitions in both switching directions, while longer times are required to reach the saturated ON and OFF current levels in the OECT device with a wider (1000 μm, figure 1(e) right) channel. The smoother (rounded shape) transitions observed in the case of the wide OECT channel design can be explained by the

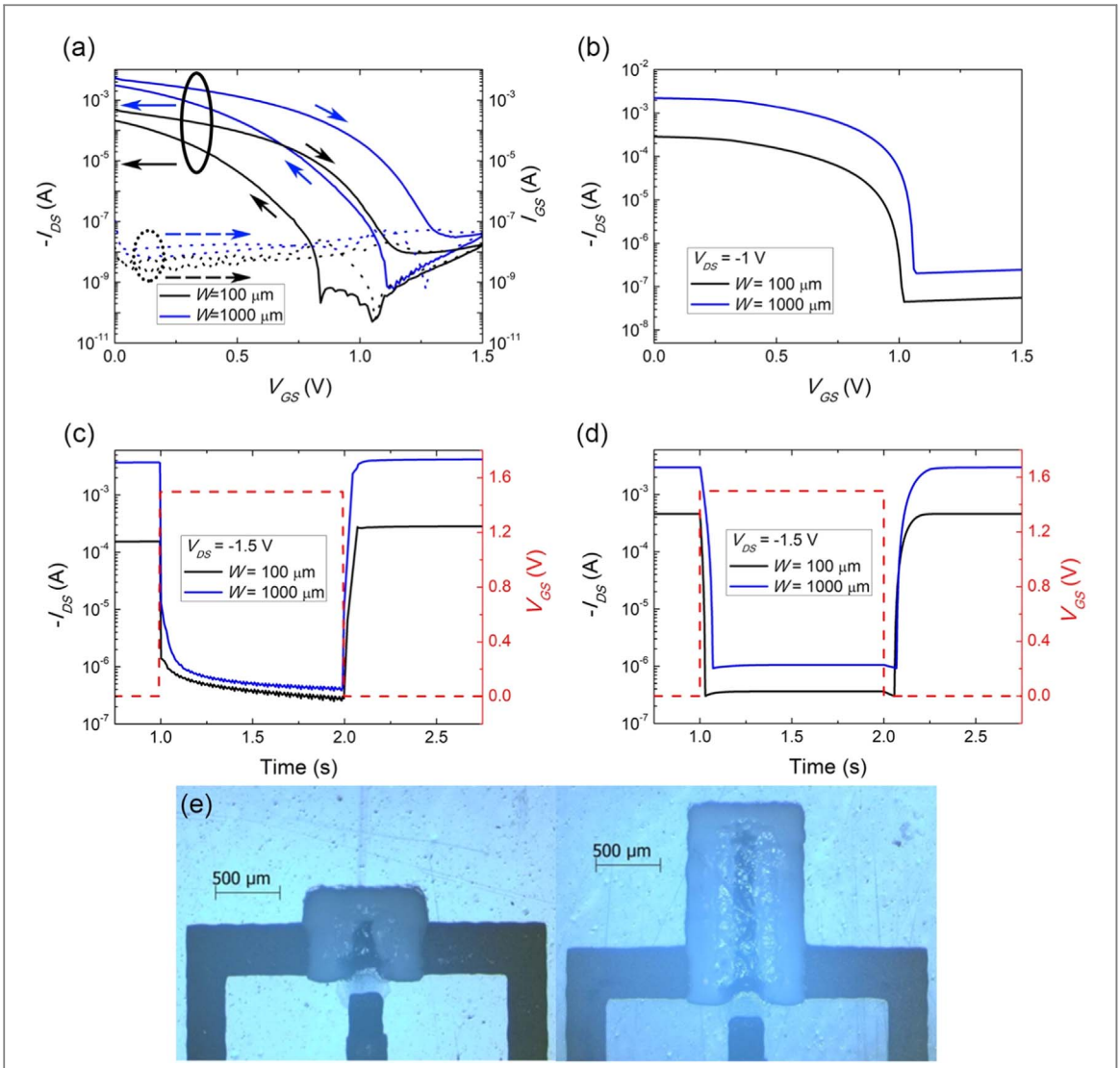

Figure 1. Transfer characteristics and dynamic switching behavior of OECTs with different channel dimensions. (a) The current throughput between the source and drain electrodes is approximately 500 μA when the channel width and length both are 100 μm (solid black line). For a channel width and length of 1000 μm and 100 μm, respectively, the current level between the source and drain electrodes is increased to approximately 5 mA, i.e. a tenfold increase in current throughput (solid blue line). Note that the switching voltage is increased by 100–150 mV, at a sweep rate of 10 mV s^{-1} and an integration time of 20 ms, this is due to the tenfold increase in charge capacity for the wide channel OECT device. The gate current contribution is denoted by a dotted line for the respective OECT architecture. (b) Simulated transfer curves of OECTs with a channel width of 100 μm (black) and 1000 μm (blue), respectively, obtained by using the SPICE model. (c) Dynamic OECT measurements, in which a constant drain-source voltage (V_{DS}) of −1.5 V and a gate voltage (V_{GS}, dashed red line) varying between 0 and 1.5 V at a frequency of 0.5 Hz are applied. The black and blue graphs denote the narrow (100 μm) and wide (1000 μm) OECT channel design, respectively. (d) Simulated dynamic switching characteristics obtained by using the SPICE model. The same OECT dimensions and applied voltages are used in (c) and (d). (e) The microscope images illustrate the two different OECT designs being evaluated. The narrow OECT design (left) is designed to have a channel width of 100 μm, while the wide OECT design (right) is designed to have a channel width of 1000 μm. Both OECT designs are designed to have a channel length of 100 μm.

increased charge capacity of the wider channel. As expected, the ON current level of the OECT with wide channel design is one order of magnitude higher as compared to the narrow one, an asset which is advantageous in display driver applications. The disadvantage is that the OFF current level also increases to some extent, which is explained by the increased area of the source and drain carbon electrodes that are exposed to the electrolyte. However, the ON/OFF ratio of the wide channel OECT design still exceeds 10^4, despite the increase in parasitic currents caused by the enlarged electrode areas.

The parasitic current also depends on the voltage applied to the OECT device. The level of the OFF current is to a large extent dependent on the voltage strain generated between the positively biased gate electrode and the negatively biased drain electrode. Hence, the required driving voltage of the load, in this case an OECD operated by an OECT-based display driver circuit, is of critical importance in order to maintain the parasitic current level at a sufficiently low level. This is further illustrated in figures 2(a) and (b), wherein the ON/OFF ratio of an OECT is reduced by approximately two orders of magnitude upon increasing the

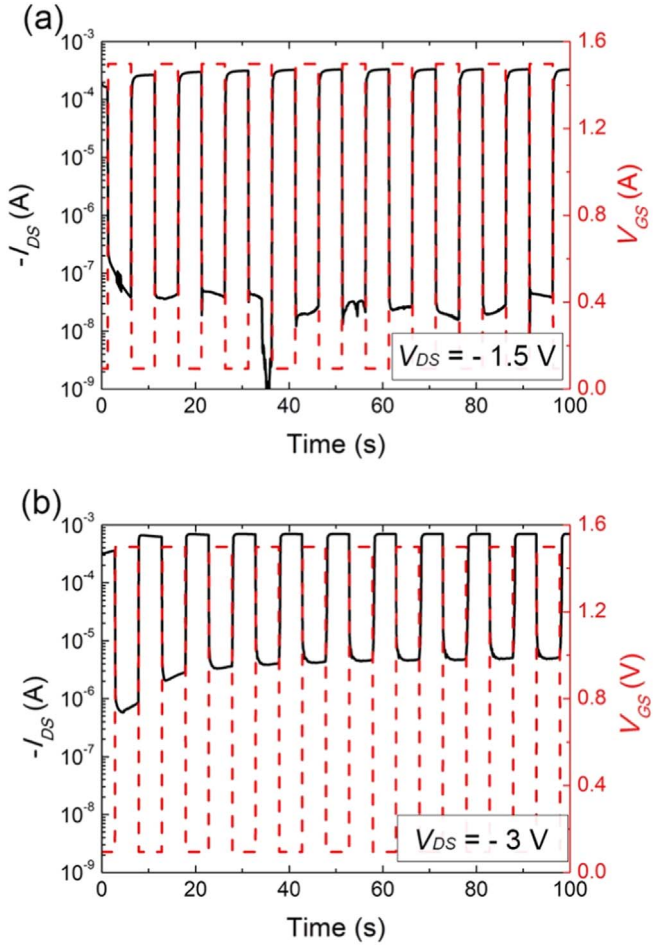

Figure 2. The dynamic switching characteristics when operating the narrow (100 μm) OECT device design at different voltage conditions. The same OECT device is used in both measurements, where V_{GS} is applied as a square wave pulse between 0.1 and 1.5 V at a frequency of 100 mHz. (a) $V_{DS} = -1.5$ V is applied to the drain electrode, which results in an ON/OFF ratio of approximately 10^4. (b) Increasing the voltage strain between the gate and drain electrodes, in this case by applying $V_{DS} = -3$ V, results in an elevated parasitic current level, and as a consequence the ON/OFF ratio is reduced to approximately 10^2.

load voltage applied at the drain electrode from −1.5 to −3 V.

3.2. Display driver circuits

The OECTs, presented here, rely on the use of the intrinsically conducting polymer PEDOT:PSS as the active channel material, and so they operate in the depletion mode. The transistor is therefore in its ON-state when a voltage close to 0 V is applied to the gate, while the channel is switched to its OFF-state upon application of $V_{GS} = 1.5$ V. This mode of operation also implies that resistor-based voltage dividers are required to enable a display driver circuit, or in fact any type of OECT-based logic circuitry based on PEDOT:PSS. Here, two different display driver circuits have been designed, screen printed and characterized. Their schematics, along with the corresponding circuit simulations, are illustrated in figure 3. The circuit schematic reported in figure 3(a) is developed for OECDs requiring the opposite voltage polarity to reverse the direction of the electrochromic switching. A voltage supply of −3 V is applied when combining this display driver circuit with the OECD requiring the opposite voltage polarity, since this will enable full color contrast and short switching time of the actual OECD, but the voltage supply can be arbitrarily selected depending on the chosen display technology. Here, the OECDs are modeled as a 47 μF capacitor ($C1$) in parallel with a 1.2 MΩ leakage resistor (R_P), see figure S2. Each branch of the circuit contains a resistor (30 kΩ) and an OECT connected in series, while the OECD bridges the two branches by a parallel connection. The conduction state of the two OECTs determines the direction of the OECD color switch, through voltage division between the resistor and the OECT channel resistance of the two different branches of the circuit. Hence, by keeping the OECTs in different conduction states, it is then possible to control the direction of the OECD charging current, which in turn results in either coloration or bleaching of the display content.

Optionally, enable signals can be implemented, e.g. by using push buttons or by incorporating two additional OECTs that bridges ground and both sides of the OECD in the parallel branch. Figure 3(b) shows a schematic of a simplified display driver circuit

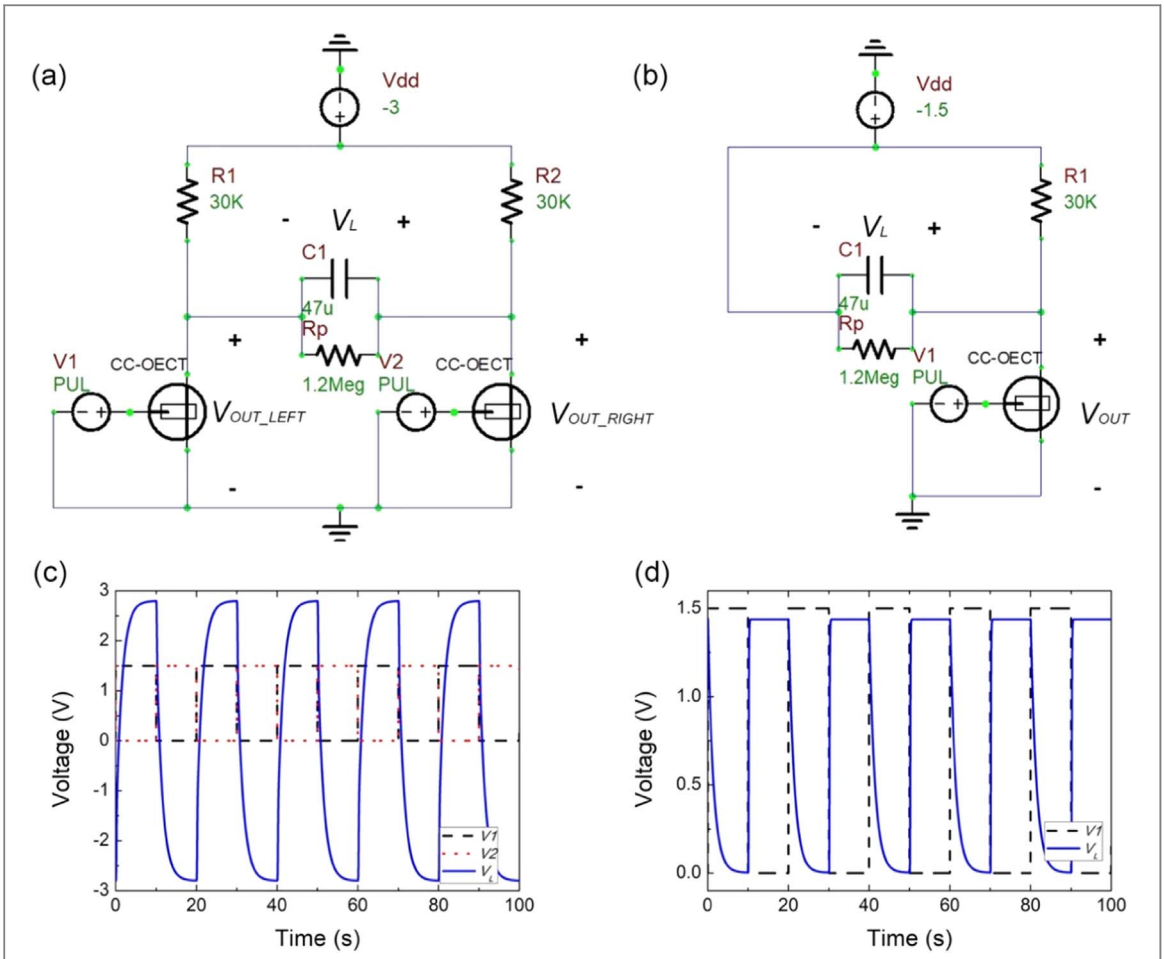

Figure 3. Two different display driver circuit designs are illustrated, along with their simulated voltage waveforms. (a) Display driver circuit for OECDs requiring the opposite voltage polarity to enable the reverse switching direction of the OECD. ±3 V are used herein as the operational voltages for this display type. (b) A simplified display driver circuit for OECDs that are spontaneously bleached upon short-circuiting the OECD, i.e. the opposite voltage polarity is not required. 1.5 V (coloration) and 0 V (bleaching) are used herein as the operational voltages for this display type. (c) Simulated voltage waveforms of the circuit shown in (a), where V_1 and V_2 are the control voltages applied to the gate electrodes of the two OECTs and V_L is the load voltage across the OECD. (d) Simulated voltage waveforms of the circuit shown in (b), where V_1 is the control voltage applied to the gate electrode of the OECT and V_L is the load voltage across the OECD.

dedicated to drive OECDs, in which the colored state can be spontaneously bleached by short-circuiting the OECD. Therefore, it is sufficient to use only one voltage division branch, while connecting the OECD in parallel to this branch. The voltage supply can be arbitrarily selected also for this display driver circuit. A voltage of −1.5 V is therefore applied in these measurements since the voltage required to obtain full color contrast is lower for this particular OECD architecture. Keeping the OECT in its conducting state, by applying a *LOW* gate voltage ($V_{GS} \approx 0$ V), results in coloration of the OECD, while the non-conducting state of the OECT ($V_{GS} = 1.5$ V) results in spontaneous bleaching of the OECD. Note that the two display driver circuits shown in figure 3 imply a trade-off; the schematic in figure 3(a) enables shorter OECD switching times in both directions, due to the elevated voltage supply (−3 V), while the lower voltage (−1.5 V) supplied to the circuit shown in figure 3(b) implies more efficient OECT switching characteristics due to the lowered level of the parasitic current generated.

Initially, standalone display driver circuits were characterized. According to the model in figure 3, a capacitor (47 μF) was used instead of the actual OECD, in order to create a circuit with similar switching characteristics. The measurements given in figures 4(a) and (b) are based on the narrow (100 μm) OECT channel, while the measurements given in figures 4(c) and (d) are based on the wide OECT channel (1000 μm). The simplified display driver circuit (figure 3(b)) is used in the measurements shown in figure 4. V_{OUT} is the actual voltage level reaching the load, in this case the capacitor, which is measured at the node between the OECT drain electrode and the resistor (figure 3(b)). The V_{OUT} level as a function of the chosen resistor value, R_1 in the display driver circuit, is evaluated in these measurements.

Results based on 5 and 30 kΩ resistors, for the respective OECT channel width, are shown in figure 4, while the measurements based on 10 and 20 kΩ resistors are presented in the supporting information (figure S3). From the result of figure 4(a) we find that a

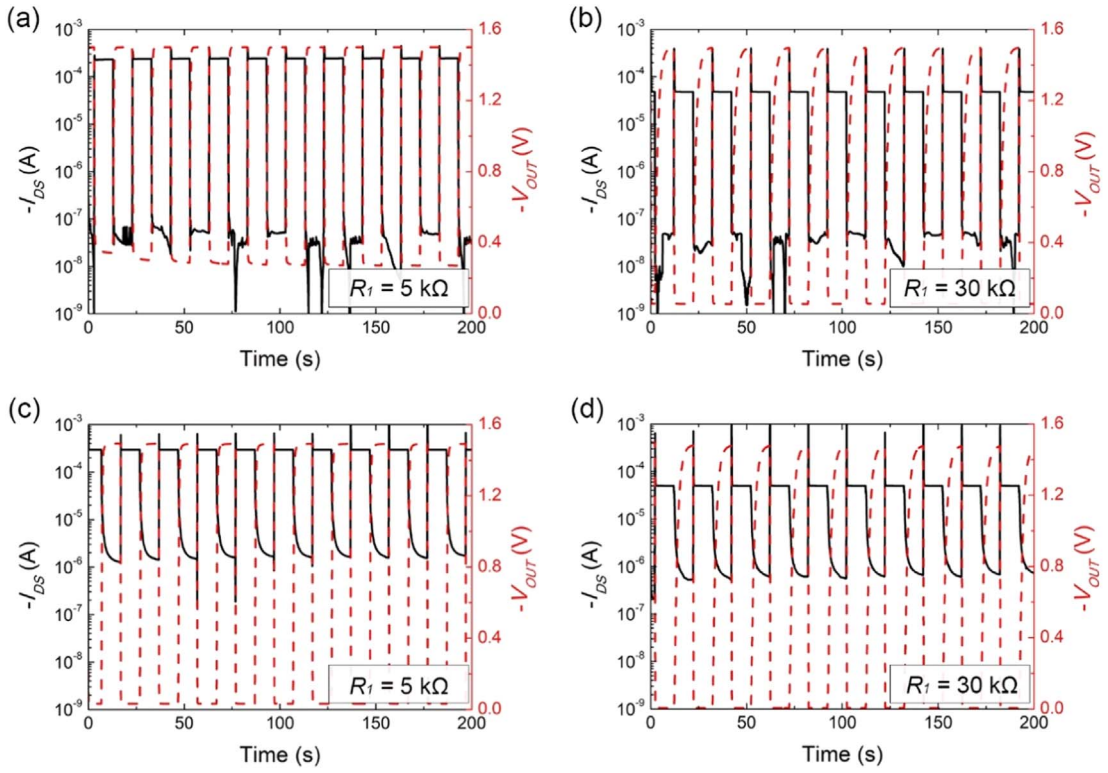

Figure 4. The switching characteristics of the display driver circuit are dependent on the chosen resistor value. The narrow OECT design (100 μm channel width) is used in (a) and (b), and the resistor value (R_1) is 5 kΩ and 30 kΩ in (a) and (b), respectively. A low resistor value results in an elevated *LOW* V_{OUT} level when the OECT channel is switched to its conducting state, which might prevent the OECD from reaching color saturation upon switching. The wide OECT design (1000 μm channel width) is used in (c) and (d), and the resistor value (R_1) is 5 kΩ and 30 kΩ in (c) and (d), respectively. The amplitudes of the V_{OUT} signal are almost independent on the value of the evaluated resistors (ranging from 5 to 30 kΩ), which is explained by the lowered ON-state resistance of the wide OECT channel design. However, both OECT channel designs result in prolonged switching times upon increasing the value of R_1.

resistor value that is too low ($R_1 = 5$ kΩ) makes it difficult to achieve $V_{OUT} \approx 0$ V, which might prevent the OECD from reaching full color contrast upon switching. On the other hand, a low resistor value results in switching characteristics of the V_{OUT} level that perfectly follow the square wave shape of the applied V_{GS}. Increasing the resistor value forces V_{OUT} towards 0 V, but this also results in a slightly prolonged switching time, as evidenced by the rounded shape of the V_{OUT} signal, see figure 4(b) for $R_1 = 30$ kΩ and figures S3(a) and (b) for the intermediate values of R_1 (10 and 20 kΩ). The OFF current levels are to a large extent unaffected by the choice of the resistor value, while the ON current levels are clearly suppressed by increased resistor values. The results presented in figures 4(c) and (d), in which the wide OECT channel design is used, show better suppression of the *LOW* V_{OUT} signal within the tested range of R_1 (5 kΩ to 30 kΩ). This is simply explained by that the channel resistance is lower when this OECT is switched to its ON-state, as compared to the narrow OECT channel design. Hence, the wide OECT channel design should be able to provide full color contrast when replacing the capacitor (47 μF) with a printed OECD. Figures S3(c) and (d) show the results when combining the wide OECT channel with the intermediate values of R_1 (10 and 20 kΩ). It can be noted that the switching time is increased, independent of the OECT channel design, when increasing the resistor values, as evidenced by the rounded shapes of the V_{OUT} signal for increased resistor values in both figures 4 and S3.

The capacitive behavior of the OECD was further investigated and the results are given in figure 5. The measurements are based on the simplified display driver circuit, shown in figure 3(b). Figure 5 shows that the switching response time is dependent on the area of the OECD that is serving as the load in the display driver circuit. Each OECD segment that is connected to the display driver circuit, in the following reported measurements, has an approximate area of 10 mm^2. Figures 5(a) and (b) refer to the narrow OECT channel design, in which either one or two OECD segments are connected to the circuit, respectively. The V_{OUT} levels are unaffected, but the switching time is prolonged when doubling the OECD area, which is explained by a twofold increase in load capacitance. The same result is obtained when a wider OECT channel design is used (figures 5(c) and (d)); the V_{OUT} levels remain unaffected, while a slightly longer switching time is observed upon doubling the display area. The chosen value of R_1 equals 10 kΩ and 5 kΩ for the circuit using the narrow and the wide OECT channel design, respectively. These resistor values were chosen since they represent a good trade-off between the levels of

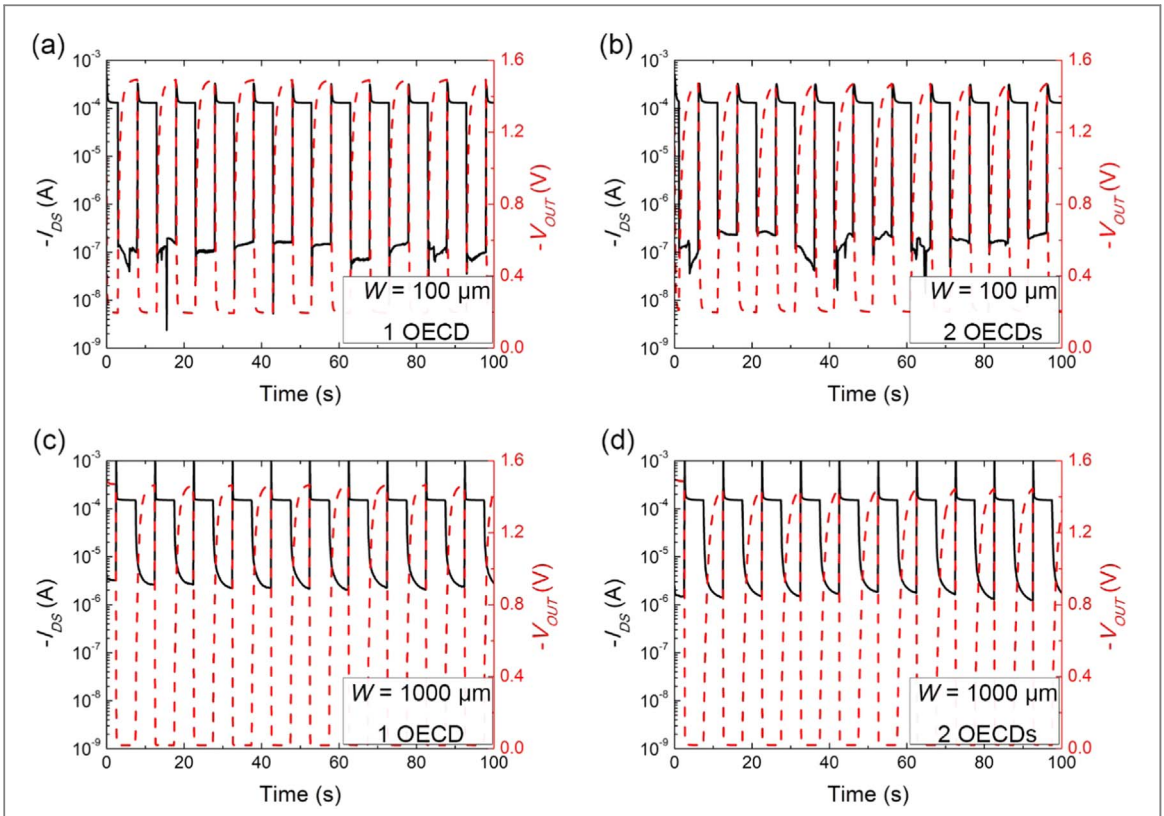

Figure 5. Switching behavior when varying the OECT channel width and the number of OECD segments connected to the display driver circuit. Narrow (100 μm) OECT channels are used in the panels shown in (a) and (b), while wide (1000 μm) OECT channels are used in the panels shown in (c) and (d). Furthermore, the (a) and (c) panels represent a load consisting of one OECD segment, while two OECD segments are used as the load in the (b) and (d) panels. The number of connected OECD segments is affecting the switching response, while the level of the V_{OUT} signal remains unaffected.

the V_{OUT} signal and the switching response time. The dependence between switching response time and the number of connected OECD segments is further demonstrated in figure S4, in which the wide OECT channel design and $R_1 = 20$ kΩ are used for all measurements, while the number of connected OECD segments is varied between one and six. Hence, increasing the display area, in this case from 10 to 60 mm^2, clearly emphasizes the dependence between load capacitance and switching response time.

The schematic in figure 3(a) has also been evaluated, even though the combination of this display driver circuit design and the OECD requiring opposite voltage polarity is less promising due to the elevated parasitic current level caused by the increased supply voltage, as shown in figure 2. One OECD segment is connected between the two branches of this circuit, in which two wide channel OECTs were used along with two 5 kΩ resistors (R_1 and R_2). Two V_{OUT} signals (V_{OUT_LEFT} and V_{OUT_RIGHT}) were recorded during the measurement, one for the respective branch (figure 3(a)), and the results are shown in figure 6. The gate voltages applied to the two OECTs of the display driver circuit are always opposite to each other, i.e. one OECT is always switched to its ON-state, while the other OECT is switched to its OFF-state, and the current is measured between the supply voltage and ground. Hence, the measured current level does not show the current modulation of each OECT, but the difference in the ON-state current throughput between the two OECTs utilized in the circuit. Ideally, if the two OECTs of the circuit have identical switching characteristics, there should be no difference in current throughput upon alternating the gate voltages, i.e. the black lines in the graphs of figure 6 would be horizontal. Both OECTs show sufficiently low resistance in their ON-state, as indicated by the very similar *LOW* V_{OUT} signals. The OECT located in the branch shown in figure 6(b) reaches a higher resistance in its OFF-state, as indicated by the fact that the *HIGH* V_{OUT} signal is closer to −3 V, as compared to the *HIGH* V_{OUT} signal shown in figure 6(a). However, despite the difference in the ON-state current throughput of the two OECTs utilized in the circuit, the OECD segment that was connected between the two branches of the circuit was switching between its fully colored and bleached states. This is explained by that the display driver circuit generated an effective OECD load voltage of almost +/−3 V upon alternating the gate voltages applied to the OECTs, as evidenced by the measured V_{OUT_LEFT} and V_{OUT_RIGHT} signals shown in figures 6(a) and (b), respectively.

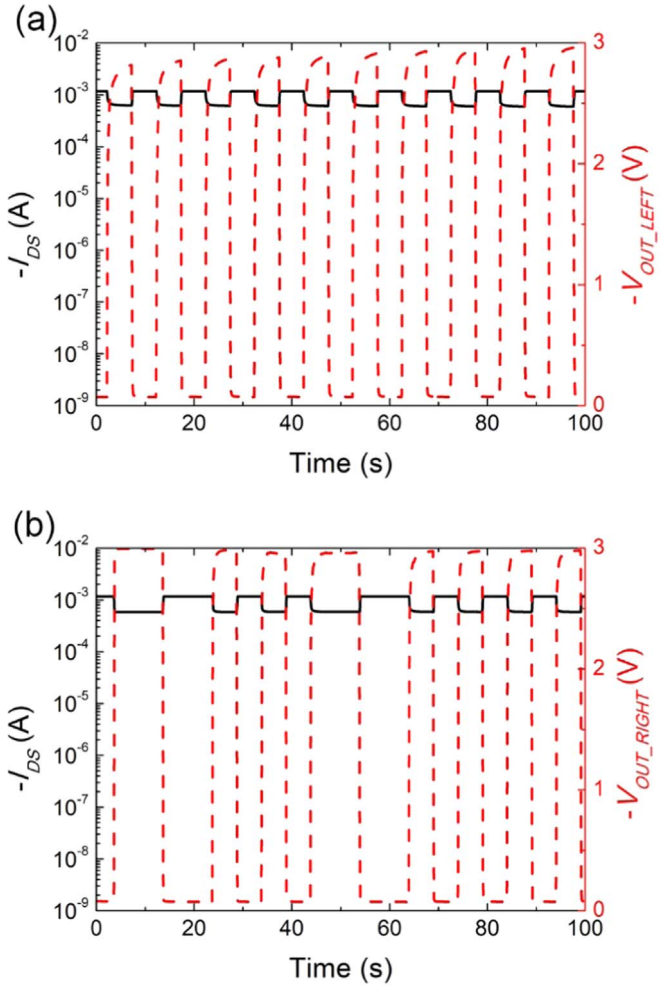

Figure 6. The display driver circuit based on two parallel branches is evaluated in this measurement, the circuit contains two wide (1000 μm) channel OECTs and two 5 kΩ resistors (R_1 and R_2). One OECD segment was connected between the two parallel branches of the circuit and −3 V was applied to the display driver circuit. By always keeping the OECTs in opposite conduction states, by applying opposite gate voltages to the OECTs, the OECD segment will switch to either its colored or bleached state. The current and voltage levels shown in (a) and (b) were measured on a respective side of the OECD.

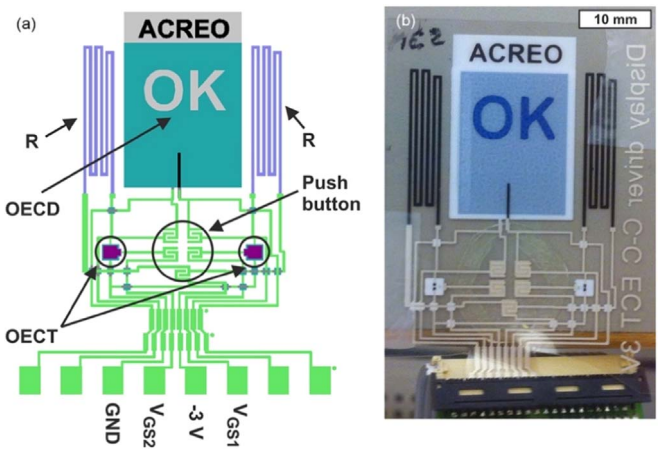

Figure 7. Screen printed and monolithically integrated display driver circuit and electrochromic display. (a) Schematic illustrating the layout of a display driver circuit monolithically integrated with an electrochromic display. (b) A photograph showing the monolithically integrated electronic system manufactured by using screen printing as the only deposition method (scale bar: 10 mm). For this particular combination of OECT control signals, full coloration of the OECD segment was obtained after also applying the enable signal by using the push button. Applying the opposite combination of OECT control signals would instead result in bleaching of the OECD segment.

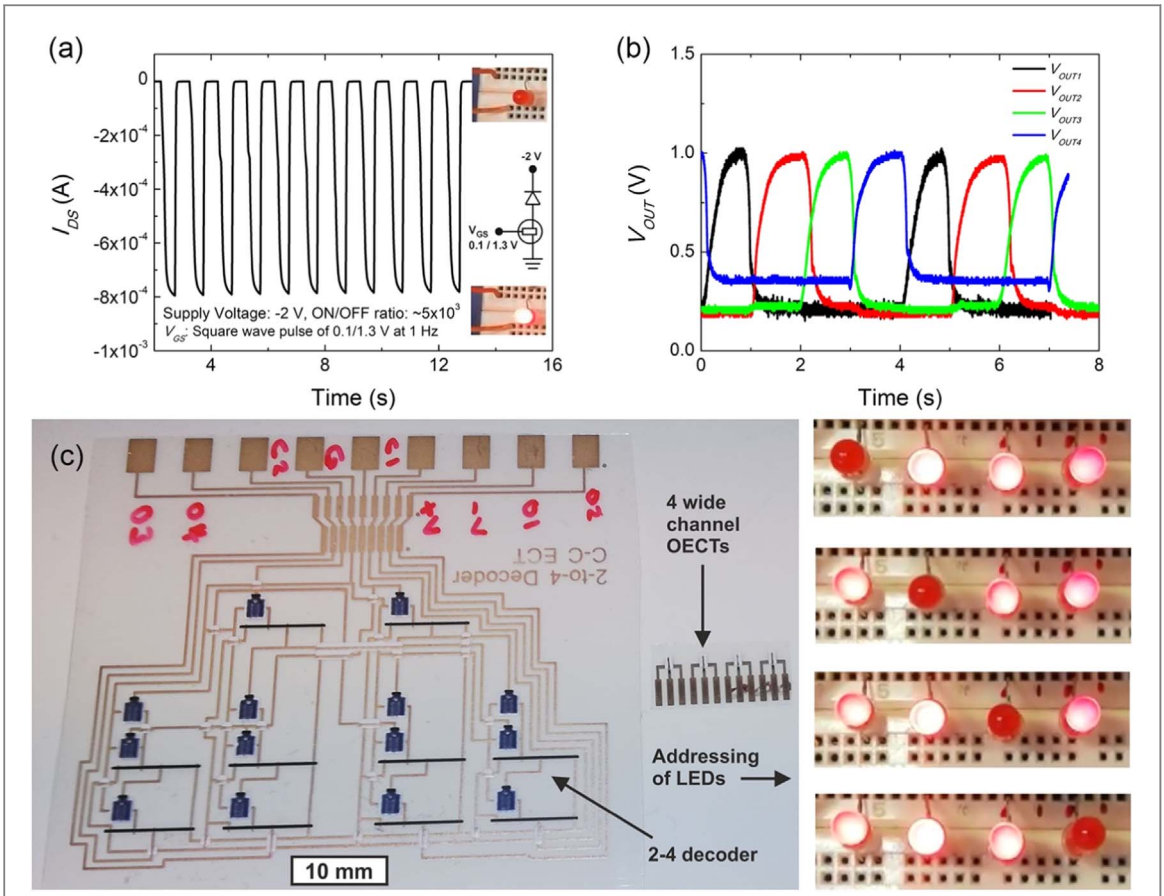

Figure 8. Wide channel OECTs and a 2–4 decoder circuit used to control the light emission from the LEDs. (a) Current versus time data when supplying −2 V to the LED cathode. The LED and a wide channel OECT are connected in series, as shown in the schematic in the inset. Hence, V_{GS} controls the light emission from the LED, which is illustrated by the inserted photographs. The V_{GS} frequency equals 1 Hz in this particular measurement, which resulted in an ON/OFF ratio of 5000 and distinguished ON and OFF states of the LED. (b) The voltage levels of the four output terminals of a 2–4 decoder circuit, showing that only one of the output terminals is allowed to be in its *HIGH* logic state for each specific voltage combination (00, 01, 10, 11) provided on the input side of the 2–4 decoder circuit. (c) Photographs (scale bar: 10 mm) showing the screen printed 2–4 decoder circuit (left), which controls the conduction state of four wide channel OECTs (middle). Each wide channel OECT is, in turn, connected in series with a corresponding LED, hence, the conduction state of the wide channel OECT controls the light emission of the LED (right). Four different combinations of light emission can be provided by the two inputs of the 2–4 decoder circuit.

3.3. Monolithic integration

Taking advantage of the fact that the OECT and OECD, here reported, both rely on the use of same materials and very similar device architectures, we then target monolithic integration of display driver circuits and electrochromic displays using screen printing as the deposition and patterning method. The circuit layout for the monolithic integration is illustrated in figure 7. The circuit relies on the design described in figure 3(a), with the only addition of an enable signal in the form of a push button. The enable signal allows pre-adjustments of the voltages (V_1 and V_2) that control the two OECTs of the circuit without affecting the color state of the OECD; the color state of the OECD is only changed upon concurrent application of V_1, V_2 and the enable signal. The resulting OECD coloration is shown in the photograph in figure 7, and the concept of OECD coloration and bleaching, depending on how the OECTs are addressed by the control signals V_1 and V_2, is further demonstrated in Video 1, see the supporting information.

3.4. Use of OECTs for high current loads

The current switching characteristics of an OECD are following the charging/discharging characteristics of a supercapacitor. The current level is high in the beginning of the charging event and then gradually attenuates exponentially. However, there are also other types of displays instead operating at constant currents, such as light emitting diodes (LEDs), that can be controlled by OECTs. Due to their electron-to-light property, LEDs constantly consume relatively high currents, typically in the mA range, a requirement that can easily be achieved by the high current throughput of the OECTs. The concept of an OECT that drives a LED device is here demonstrated, see figure 8(a). A red LED is here connected in series with the wide channel OECT. A voltage of −2 V is supplied to the LED cathode, and the light emission is thus controlled by applying V_{GS}, varied between 0.1 and 1.3 V, to the OECT gate electrode. When the gate voltage is pulsed at a frequency of 1 Hz, an ON/OFF ratio of approximately 5000 is attained. The ON/OFF ratio gradually decreases as the frequency of V_{GS} increases,

due to the relatively slow switching response of the OECT device. ON/OFF ratios of 10 000, 5000, 1750, 400, 30 and 4 are obtained for V_{GS} operating at frequencies of 0.5, 1, 2, 5, 10 and 20 Hz, respectively. However, despite the very low ON/OFF ratio at 20 Hz, the LED blinking effect is still clearly observed. This is further demonstrated in Video 2 (V_{GS} switches at 1 Hz) and Video 3 (V_{GS} switches at 10 Hz), see the supporting information.

Figure 8(b) presents the voltage levels measured at the four output terminals of a screen printed 2–4 decoder circuit, upon providing the input sequence [00, 01, 10, 11] as addressing signals to the decoder circuit. The input sequences are changed at a frequency of 1 Hz, and the truth table of the 2–4 decoder circuit is revealed by monitoring the voltage levels at the output terminals. Each input combination (e.g. '00') only allows its corresponding output terminal (e.g. V_{OUT1}) to be in its *HIGH* logic state [27]. Decoders can be used to address an electronic circuit containing multiple LEDs, and thereby controlling the light emission. Each output terminal of the 2–4 decoder circuit was then connected to the gate electrode of a corresponding wide channel OECT, which in turn was connected in series with a corresponding LED. The 2–4 decoder circuit, the wide channel OECTs here used to control the light emission, and photographs of a full update sequence are given in figure 8(c). Additionally, an update sequence at 1 Hz is also demonstrated in Video 4 in the supporting information.

4. Conclusions

In summary, we have reported on the topic of developing and applying OECT-based display driver circuits, to control the information content in OECDs and LEDs. Two different display driver circuits, each combined with a corresponding OECD device, were developed and evaluated through measurements and SPICE simulations. The fundamental device structures of the OECTs and OECDs are based on the interface between an electrolyte and an organic semiconductor and, in fact, rely on the very same combination of materials and low-voltage switching mechanism. Hence, this allows for the development of a simplified manufacturing approach including concurrent processing of OECTs and OECDs, which in this case relies entirely on screen printing as the deposition and patterning method of all the materials required for the completion of devices and circuits. The manufacturing approach is successfully verified through operation of OECT-based display driver circuits, monolithically integrated with OECDs. The resulting OECT and OECD devices are controlled through the application of low voltages, typically within the range 1–3 V. Despite the low-voltage operation, a current throughput of several mA is easily obtained in all-screen printed OECTs, owing to that charge transport occurs throughout the entire PEDOT:PSS bulk channel that bridges the source and drain electrodes. The high current throughput is demonstrated by utilizing OECTs to control the light emission in LEDs, where the actual LED addressing is achieved by an OECT-based decoder circuit. The all-screen printed technology presented herein, in which OECTs and OECDs are monolithically integrated and manufactured on flexible plastic foils, paves the way for printed electronics in biosensor platforms for distributed healthcare, sensor platforms for monitoring of arbitrary sensors, electronic smart labels within packaging, and other IoT applications targeted in the future.

Acknowledgments

This project was financially supported by the Swedish Foundation for Strategic Research (Silicon-Organic Hybrid Autarkic Systems, project ID: SE13-0045), H2020-EU.2.1.1 (WEARPLEX, project ID: 825339) and EUREKA Eurostars (PROLOG, project ID: 7301). The authors would like to thank Dr Xin Wang at RISE Acreo for optical profilometer measurements of the thickness and roughness of the printed layers.

ORCID iDs

Peter Andersson Ersman https://orcid.org/0000-0002-4575-0193
Simone Fabiano https://orcid.org/0000-0001-7016-6514

References

[1] Nathan A *et al* 2012 Flexible electronics: the next ubiquitous platform *Proc. IEEE* **100** 1486–517
[2] Inganäs O 2018 Organic photovoltaics over three decades *Adv. Mater.* **30** 1800388
[3] Liu L, Feng Y and Wu W 2019 Recent progress in printed flexible solid-state supercapacitors for portable and wearable energy storage *J. Power Sources* **410–411** 69–77
[4] Crone B *et al* 2000 Large-scale complementary integrated circuits based on organic transistors *Nature* **403** 521–3
[5] Berggren M and Richter-Dahlfors A 2007 Organic bioelectronics *Adv. Mater.* **19** 3201–13
[6] Andersson P *et al* 2002 Active matrix displays based on all-organic electrochemical smart pixels printed on paper *Adv. Mater.* **14** 1460–4
[7] Berggren M, Nilsson D and Robinson N D 2007 Organic materials for printed electronics *Nat. Mater.* **6** 3–5
[8] Lee S M, Kwon J H, Kwon S and Choi K C 2017 A review of flexible OLEDs toward highly durable unusual displays *IEEE Trans. Electron Devices* **64** 1922–31
[9] Street R A *et al* 2006 Jet printing flexible displays *Mater. Today* **9** 32–7
[10] Cao X *et al* 2016 Fully screen-printed, large-area, and flexible active-matrix electrochromic displays using carbon nanotube thin-film transistors *ACS Nano* **10** 9816–22
[11] Kawahara J *et al* 2013 Flexible active matrix addressed displays manufactured by printing and coating techniques *J. Polym. Sci. B* **51** 265–71

[12] Borchardt J K 2004 Developments in organic displays *Mater. Today* **7** 42–6
[13] Kumar A and Zhou C 2010 The race to replace tin-doped indium oxide: which material will win? *ACS Nano* **4** 11–4
[14] Han T H *et al* 2016 Approaching ultimate flexible organic light-emitting diodes using a graphene anode *NPG Asia Mater.* **8** e303
[15] Mortimer R J 1999 Organic electrochromic materials *Electrochim. Acta* **44** 2971–81
[16] Kobayashi N, Miura S, Nishimura M and Urano H 2008 Organic electrochromism for a new color electronic paper *Sol. Energy Mater. Sol. Cells* **92** 136–9
[17] Invernale M A, Ding Y and Sotzing G A 2010 All-organic electrochromic spandex *ACS Appl. Mater. Interfaces* **2** 296–300
[18] Andersson Ersman P, Kawahara J and Berggren M 2013 Printed passive matrix addressed electrochromic displays *Org. Electron.* **14** 3371–8
[19] Fabiano S *et al* 2017 Ferroelectric polarization induces electronic nonlinearity in ion-doped conducting polymers *Sci. Adv.* **3** e1700345
[20] Aerts W F, Verlaak S and Heremans P 2002 Active-matrix OLED display *IEEE Trans. Electron Devices* **49** 2124–30
[21] Gelinck G H *et al* 2004 Flexible active-matrix displays and shift registers based on solution-processed organic transistors *Nat. Mater.* **3** 106–10
[22] Furno M, Kleemann H, Schwartz G and Blochwitz-Nimoth J 2015 Vertical organic transistors (V-OFETs) for truly flexible AMOLED displays *SID Symp. Dig. Tech. Pap.* vol 46, pp 597–600
[23] Rivnay J, Inal S, Salleo A, Owens R M, Berggren M and Malliaras G G 2018 Organic electrochemical transistors *Nat. Rev. Mater.* **3** 17086
[24] Mach P, Rodriguez S J, Nortrup R, Wiltzius P and Rogers J A 2001 Monolithically integrated, flexible display of polymer-dispersed liquid crystal driven by rubber-stamped organic thin-film transistors *Appl. Phys. Lett.* **78** 3592–4
[25] Zhou L, Wanga A, Wu S C, Sun J, Park S and Jackson T N 2006 All-organic active matrix flexible display *Appl. Phys. Lett.* **88** 083502
[26] Andersson Ersman P *et al* 2019 All-printed large-scale integrated circuits based on organic electrochemical transistors *Nat. Commun.* **10** 5053
[27] Andersson Ersman P *et al* 2017 Screen printed digital circuits based on vertical organic electrochemical transistors *Flex. Print. Electron.* **2** 045008